JGR Biogeosciences

RESEARCH ARTICLE
10.1029/2018JG004787

Pyrogenic carbon erosion after the Rim Fire, Yosemite National Park: The Role of Burn Severity and Slope

Rebecca B. Abney[1], Timothy J. Kuhn[2], Alex Chow[3], William Hockaday[4], Marilyn L. Fogel[1,5], and Asmeret Asefaw Berhe[1]

[1]Environmental Systems, Life and Environmental Sciences, University of California, Merced, CA, USA, [2]Yosemite National Park, National Park Service, Yosemite, CA, USA, [3]Forestry and Environmental Conservation Department, Clemson University, Clemson, SC, USA, [4]Department of Geosciences, Baylor University, Waco, TX, USA, [5]Department of Earth Science, University of California, Riverside, CA, USA

Key Points:
- Sediment eroded from moderate burn severity areas was composed of more unburned, fresh organic matter
- Sediment eroded from high severity burn areas was enriched in pyrogenic carbon compared with that from moderate burn severity sediment
- Burn severity played a primary role in controlling PyC transport after the Rim Fire, while slope angle played a secondary role

Correspondence to:
R. B. Abney,
rebabney@iu.edu

Citation:
Abney, R. B., Kuhn, T. J., Chow, A., Hockaday, W., Fogel, M. L., & Berhe, A. A. (2019). Pyrogenic carbon erosion after the Rim Fire, Yosemite National Park: The role of burn severity and slope. *Journal of Geophysical Research: Biogeosciences*, *124*. https://doi.org/10.1029/2018JG004787

Received 5 SEP 2018
Accepted 26 JAN 2019
Accepted article online 1 FEB 2019

Abstract Pyrogenic carbon (PyC) is an incomplete combustion by-product with longer soil residence times compared with nonpyrogenic components of the soil carbon (C) pool and can be preferentially eroded in fire-affected landscapes. To investigate geomorphic and fire-related controls on PyC erosion, sediment fences were established in three combinations of slope (high 13.9–37.3%; moderate 0–6.7%) and burn severity (high; moderate) plots within the perimeter of the Rim Fire in 2013, Yosemite National Park, California, USA. After each major precipitation event following the fire, we determined transport rates of total sediment, fine and coarse sediment fractions, and C and nitrogen (N). We measured stable isotope ($\delta^{13}C$ and $\delta^{15}N$) compositions and ^{13}C-nuclear magnetic resonance spectra of soils and eroded sediments. The highest total and fine (<2 mm) sediment transport in high severity burned areas correlated with initial discharge peaks from an adjacent stream, while moderate burn severity sites had considerably more of the >2 mm fraction transported than high burn severity sites. The $\delta^{13}C$ and $\delta^{15}N$ values and ^{13}C-nuclear magnetic resonance analyses indicated that sediment eroded from moderate severity burn areas included fresh organic matter that was not as significantly affected by the fire, whereas sediments from high severity burn areas were preferentially enriched in PyC. Our results indicate that along a single hillslope after the Rim Fire, burn severity acted as a primary control on PyC transport postfire, with slope angle likely playing a secondary role. The preferential erosion of PyC has major implications for the long-term persistence of PyC within the soil system.

1. Introduction

Fire and erosion can have multiple independent and interactive effects on soil health, plant productivity, and biogeochemical cycling of C, N, and other essential nutrients. Little is known about how the interactions of complex topography and changes in soil properties due to fire (i.e., loss of vegetative plant and litter cover and increased hydrophobicity in topsoil) can affect postfire soil carbon (C) and overall terrestrial organic matter (OM) dynamics. These interactions are particularly crucial since the terrestrial biosphere is dominated by sloping landscapes (Staub & Rosenzweig, 1992), and postfire soil erosion plays critical roles in controlling soil chemical and physical properties, biogeochemical processes within the soil system, and the flux of elements from terrestrial to aquatic systems (Berhe et al., 2012, 2018; Doetterl et al., 2016; Harden et al., 1999; Stallard, 1998). Furthermore, around 450 Mha of the globe is impacted by fire annually (Randerson et al., 2012). Hence, when fires and erosion overlap in space and time, their interactive effects on lateral redistribution of nutrients and OM postfire (Abney et al., 2017) impose important controls on the available nutrients for postfire regrowth (Certini, 2005; Johnson et al., 2007).

1.1. Erosion and SOM Dynamics

Erosion globally redistributes 75 Gt of soil and 1- to 5-Gt soil organic carbon annually (Battin et al., 2009; Berhe et al., 2007; Regnier et al., 2013; Stallard, 1998). Erosional redistribution of topsoil affects numerous processes in the source catchments and moves soil, C, N, and other nutrients from terrestrial to aquatic ecosystems (Berhe et al., 2018). About 70–90% of that eroded material is redistributed downhill or downstream but is not exported out of the source watershed (Gregorich et al., 1998; Lal, 2003; Rumpel et al., 2006). In upslope eroding landform positions, erosion leads to a loss of soil organic matter (SOM)

from soil profiles through direct removal of soil mass. In contrast, in depositional landform positions, erosion leads to input and stabilization of at least some of the SOM through processes including the following: (1) enhanced rates of plant productivity in depositional landform positions, (2) new and reconfigured associations of the eroded SOM with soil minerals, and (3) burial from subsequently eroded material (Berhe et al., 2012; Sharpley, 1985). When considered at the watershed scale, and accounting for the replacement of eroded OM by production of new photosynthate in eroding slopes and the stabilization of some eroded OM in depositional settings, soil erosion and deposition act together to induce a net terrestrial sink of 0.12–1.5 Gt C/year, (Berhe et al., 2007, 2008; Harden et al., 1999; Stallard, 1998; Van Oost et al., 2007).

1.2. Fire and SOM Dynamics

One of the major by-products of fire is pyrogenic carbon (PyC), which results from the incomplete combustion of biomass and includes a range of products such as ash, charcoal, and charred biomass (Bird et al., 2015; Masiello, 2004). In the soil system, PyC is persistent, with reported mean residence times ranging from centuries to millennia (Bird et al., 2015; Hammes et al., 2007, 2008; Lehmann, 2007; Lehmann et al., 2008). Additionally, PyC has a high surface area, which allows it to have higher reactivity compared with nonpyrogenic C, and has been shown to serve as a sorbent for SOM (Chia et al., 2012; Cornelissen et al., 2005; Mukherjee et al., 2011). Condensation of volatile organic compounds during moderate to low combustion temperatures (~175–250 °C) also renders soil more hydrophobic compared to unburned soil, and at higher combustion temperatures, the hydrophobic layer can be either pushed deeper into the soil or destroyed (DeBano, 2000; Doerr et al., 2004; Mataix-Solera et al., 2011; Shakesby & Doerr, 2006). The properties of PyC depend heavily on combustion conditions, including temperature, oxygen availability, fuel type and conditions, and duration, with higher temperatures leading to increased aromatic condensation and loss of oxygenated functional groups (Bird et al., 2015; Masiello, 2004). Furthermore, the charring of SOM and formation of PyC in mineral soil also depends on combustion conditions, in addition to preexisting soil properties (Araya et al., 2017, 2016; Certini, 2005).

1.3. Significance and Effects of PyC Erosion

There are numerous complex interactions between fire and erosion, and the extent of these interactions depends on fire severity, postfire management, climate (Certini, 2005), and rate of vegetation recovery (Baker, 1988), among other factors. Erosion, in turn, can indirectly affect vegetation and soil moisture content. Both fire and erosion are controlled by climate to various extents (Imeson & Lavee, 1998; Neary et al., 1999; Riebe et al., 2001). The size of watershed and topography (Iniguez et al., 2008; Liu et al., 2003) and amount, intensity, and temporal distribution of precipitation can influence the rate of bulk SOM and PyC loss from or redistribution within an eroding watershed (Cain et al., 1999; Nearing, 1998). Many erosion prediction models, such as the Universal Soil Loss Equation (Wischmeier & Smith., 1965, 1978), have confirmed the importance of slope and topographic characteristics for soil erosion, which have also been widely studied in field settings (Assouline & Ben-Hur, 2006; Cerdà & García-Fayos, 1997; Chaplot & Le Bissonnais, 2000).

Numerous properties of PyC make it highly susceptible to erosion (Rumpel et al., 2006, 2015). The majority of PyC is produced and deposited on the soil surface, which is the first material to erode from a hillslope. During low- to moderate-temperature combustion, hydrophobic layers can form beneath the soil surface, leading to decreases in the infiltration rate of water (DeBano, 2000; DeBano et al., 1998; Doerr & Thomas, 2000; Robichaud, 2003). The low density of PyC and its hydrophobic properties when formed at lower temperatures (Sander & Pignatello, 2005) also increase the likelihood for it to be transported by flowing water by, for example, saturation overland or Hortonian flows (Shakesby & Doerr, 2006). These properties can interact to make PyC susceptible to preferential erosion over nonpyrogenic material.

A handful of previous studies (Cotrufo et al., 2016; Rumpel et al., 2009, 2006; Saiz et al., 2018) have provided direct evidence for the preferential erosion of PyC postfire in smaller plots in agricultural and natural soils. However, as of yet, the relative rates of PyC versus bulk SOM erosion at the scales of plots, hillslopes, or watersheds remain relatively unexplored, particularly after wildfires (Abney & Berhe, 2018; Abney et al., 2017). Our investigation seeks to determine how and if the preferential erosion of PyC is a function of both the properties of the PyC, as a function of burn severity, or PyC formation conditions, as well as the timing and magnitude of erosion events at the hillslope scale.

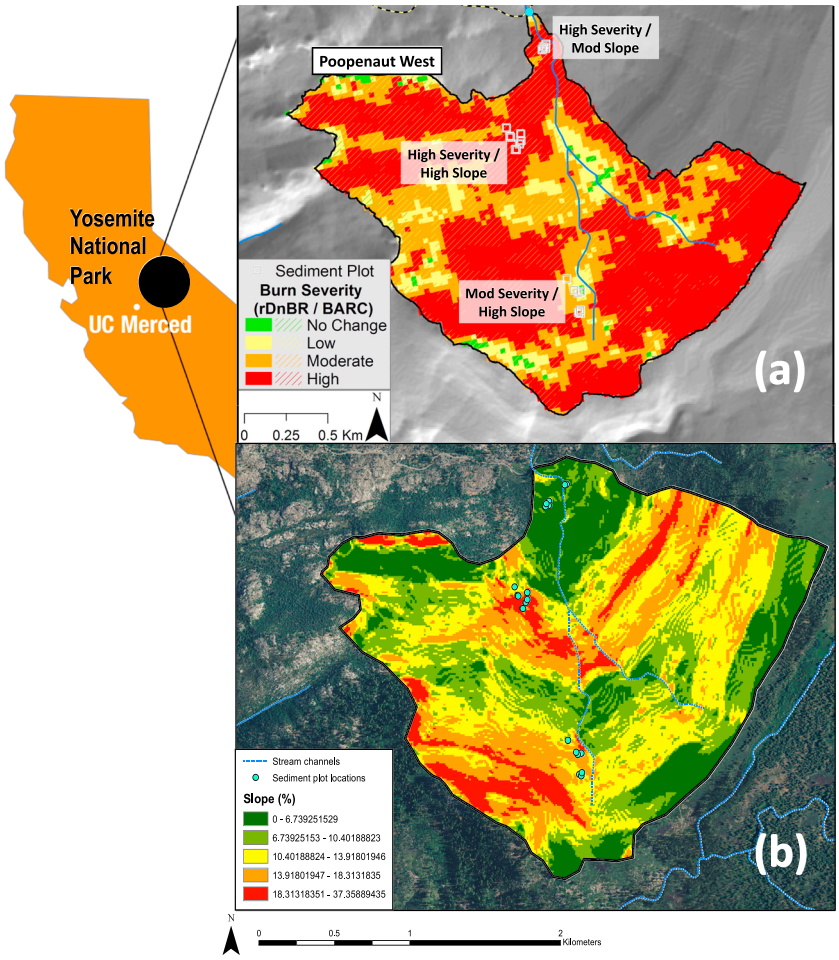

Figure 1. Soil burn severity and slope in the Poopenaut watershed within Yosemite National Park. The 21 sediment plots are denoted by gray squares and were chosen based on combination of fire severity (a) and slope (b). The Poopenaut watershed is near the Hetch Hetchy entrance to Yosemite National Park. BARC = Burned Area Reflectance Classification.

1.4. Research Objectives

This project aims to understand how the interaction of burn severity and slope control erosional transport of OM (total SOM and PyC) in upland temperate forest ecosystems. Specifically, we determine (a) how slope and fire severity interact to control transport of different soil constituents (i.e., fine and coarse sediments, soil C, N, and PyC concentration in sediments) and (b) how fire severity controls nature of bulk C and PyC mobilized by erosion.

2. Methods

2.1. Study Site

This study was conducted in the Sierra Nevada mountain range of California, in the area affected by the Rim Fire in 2013. The Rim Fire burned over 1,000 km^2 land from August to November of 2013, in an area that covered parts of Yosemite National Park and Stanislaus National Forest. The specific study watershed used in this study is Poopenaut West, which is located within Yosemite National Park, in a subwatershed of the Tuolumne River basin. The watershed has a mean annual precipitation of 915 mm. For the 1-year study period, the Tuolumne River basin was at 58% of average precipitation (California Data Exchange Center, 2016), and the watershed was under transitive snow cover from the time of burn containment to initial sampling.

Sites were selected along a single hillslope in a watershed within the perimeter of the Rim Fire, near the Hetch Hetchy entrance to Yosemite National Park, with elevations ranging from 1,475 to 1,740 m above

Figure 2. Photo of Poopenaut West watershed inside the perimeter of the Rim Fire from 4 March 2014, 3-month postfire. The dashed line delineates the boundary between high (a) and moderate (b) severity burn areas (Photo Credit: R. Abney).

sea level (Figure 1). Holocene era granitic glacial deposits underlie the study area (N. K. Huber et al., 1989), and the soils are dominated by coarse loamy, isotic, frigid Typic Dystroxerepts; coarse loamy, isotic, frigid Humic Dystroxerepts; and coarse loamy, isotic, mesic Typic Dystroxerepts (United States Department of Agriculture, 2007). The study area is a mixed conifer forest, with *Pinus jeffreyi*, *Pinus ponderosa*, *Ceanothus* spp., and *Manzanita* spp.

Vegetation and soil burn severity were assessed using the Burned Area Reflectance Classification, which assesses the infrared reflectance of a landscape in comparison to references (Hudak et al., 2014), and this burn classification was ground truthed to these sites to create a soil burn severity map (Parsons et al., 2010). Thresholds in the relative differenced normalized burn ratios in the BARC classification are: moderate < 500; and high > 500. Burn severity and slope angle (Figure 1) were used to select sites that varied on burn severity and slope. We set up sampling areas in three classification groups: (a) *HH*: high severity burn, high slope (26–41°); (b) *HM*: high severity burn, moderate slope (5–23 °); and *MH*: moderate severity burn, high slope (21–27°). Sites were selected along the same hillslope in forested areas with similar vegetation cover. There was approximately 1 km between the furthest two sites. The major difference we observed among the three classification groups was the proportion of remaining vegetation (Figure 2). The high severity burn areas were completely devoid of vegetation cover, mainly leaving behind burned tree trunks and exposed soil surfaces overlain by a patchy, and occasionally several centimeters thick, cover of a mixture of charcoal and ash, as defined by Bodí et al. (2014), much of which was mobilized after the initial erosion event. In the moderate severity burned areas, a considerable number of trees survived the fire, leaving 65% canopy cover compared with <30% canopy cover in high severity burn sites and hence, the groundcover constituted a mixture of charred and fresh litter that presumably fell after the fire.

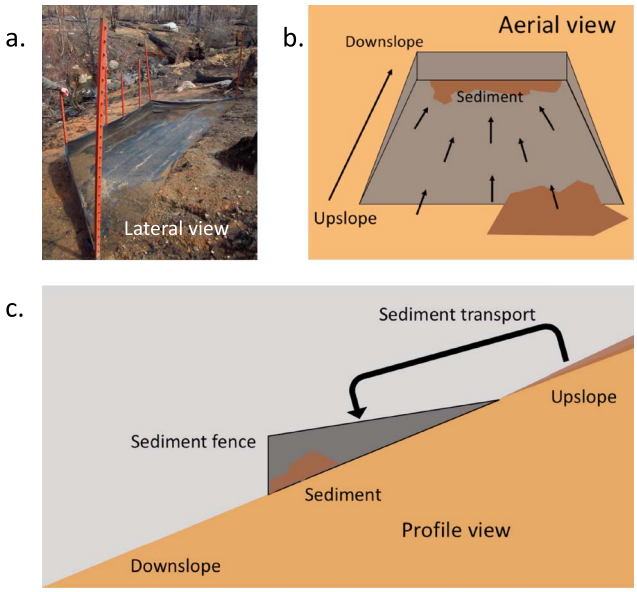

Figure 3. Sediment fences were established alongside a single hillslope in the Poopenaut West watershed. Photo (a) is from February 2014 within the high burn severity moderate slope sampling area. During precipitation events, upslope sediment was washed into the sediment fences (b and c). Sediment fences were swept after every major precipitation event in the watershed.

2.2. Field Sampling Methods

The sites we selected burned on 25 August 2013, and sediment fences were established in November of 2013 by staking down a water-permeable tarp with rebar parallel to the hillslope, and the upslope source area was delineated with trenches to prevent erosion of material from further upslope or adjacent locations. Seven sediment fences were established within each classification group ($n = 3$) for a total of 21 fences (Figure 3). After installation, sediment fences were cleared from any eroded sediment prior to 26 November 2013, which was the initiation of data collection. Prior to setting up sediment fences, four precipitation events occurred in the Poopenaut watershed. Source areas for sediment catchments were approximately 100 m^2, with dimensions of 20 m long and 5 m wide. Sediments within these fences were sampled after every precipitation event postfire beginning after spring snowmelt, with a total of four precipitation events during the water year of 2014 and 84 sediment samples (see Figure 4). The initial water year samples from this study were used for detailed physicochemical analyses as presented in this study to capture the initial, rapid, and often preferential transport of SOM postfire. Precipitation events were monitored via a tipping bucket rain gauge located in the Poopenaut West stream that flows below the sediment fences (Figure 1 and Table 1). Sediment was allowed to dry for several days within the fence and was collected by sweeping the entire fenced area with a broom until it was cleared. Once collected, the sediment was

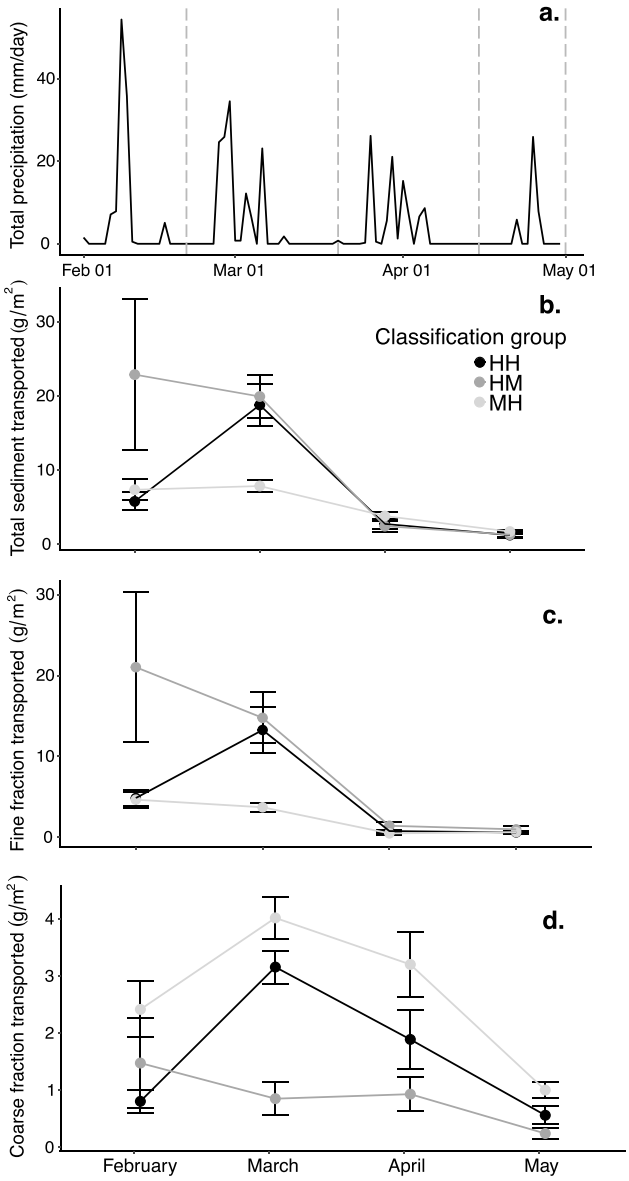

Figure 4. Precipitation was summed per day, and sediment sampling occurred after major precipitation events (a, dashed gray lines indicate dates of the four sampling points). The total sediment (b) transported during each sampling event was weighed and dried from each of the three classification groups (HH = high burn severity, high slope; HM = high burn severity, moderate slope; and MH = moderate burn severity, high slope). The sediment was sieved into fine (<2 mm, c) and coarse (>2 mm, d) fractions. The sampling points represent sediment transported from precipitation events prior to the sampling point and are presented as mean with standard error per classification group (n = 7).

weighed, and dry sediment mass was determined by gravimetrically correcting for water content by drying subsamples of the sediments in the oven for 24 hr at 105 °C.

Soils were collected during March of 2014, concurrent with the second sediment collection, from the area directly upslope from the marked source material for the sediment fence areas that represent putative source soils for the material eroded into the sediment fences. Soils were collected from three randomly selected sites to capture the variability of the soil and within a meter of the source area perimeter and at least a meter apart from each other. Soils were collected at each sediment fence from each treatment group, for a total of 63 soil samples. Soils were collected using a closed bucket metal auger with a 5-cm-diameter plastic sleeve and capped after removal from the ground. Soils were kept on ice until returning to the laboratory, where they were stored at 4 °C until further analysis. Soils were separated into depths of 0–5 and 5–10 cm in the laboratory.

2.3. Laboratory Analysis

Additionally, *P. ponderosa* litter and duff were collected from unburned forest near the Rim Fire affected area immediately after the fire (November 2013). This litter was collected to assess the changes in litter chemistry with increasing charring temperature. The litter was charred under no oxygen, pyrolysis conditions in a furnace at two temperatures (250 °C, 550 °C), with a sample dried at 50 °C as a control, for an hour to determine how fire temperature controls the nature of the OM that is typically found on the soil surface postfire. Previous research demonstrated that wildfire and laboratory generated chars differ significantly in various chemical properties (Santín et al., 2017); however, this charring sequence is specific to and representative of the litter charred within this site.

Field-moist sediment and source soil samples were passed through a 2-mm sieve (defined as coarse and fine fractions). The <2-mm fraction was analyzed for pH in both deionized water and 0.01M $CaCl_2$ 1:2 soil (sediment):solution mass ratio (Hendershot et al., 2008; Schofield & Taylor, 1955). We determined particle size distribution via the hydrometer method (Bouyoucos, 1962) and bulk density of the source area soils using the core method (Blake & Hartge, 1986). Soils and sediments were tested for the presence of carbonates using 1 M HCl, and no carbonates were found in any sample.

A representative subsample of the sieved <2 mm fraction of the soil and sediment samples was air-dried and ground using a SPEX Mill (SPEX Sample Prep, Metuchen, NJ, USA). Carbon and nitrogen concentrations, as well the $\delta^{13}C$, and $\delta^{15}N$ values of these samples, were determined on a Costech ECS 4010 CHNSO Analyzer interfaced with a Conflo IV interface to a Delta V Plus Isotope Ratio Mass Spectrometer at UC Merced's Stable Isotope Laboratory. Approximately 7 mg of air-dried sample was weighed into 4 × 6-mm tin capsules. The samples were measured relative to an acetanilide standard and a laboratory soil internal standard. These internal standards were compared with international standards: atmospheric N for the $\delta^{15}N$ standard and to Vienna Pee Dee Belemnite for the $\delta^{13}C$. Standards were measured in triplicate with precision of ±1.84% C, 0.29% N, 0.77‰ $\delta^{13}C$, and 0.09‰ $\delta^{15}N$. Samples were measured in triplicate with precision of ±0.80% C, 0.02% N, 0.07‰ $\delta^{13}C$, and 0.02‰ $\delta^{15}N$. Sample error was likely smaller than the standard error due to the considerably larger number of standard replicates that were run. Concentrations of C and N were corrected to air-dry weights by oven-drying previously air-dried,

Table 1
Precipitation Totals and Peaks From the Nearby Poopenaut Valley for the Spring 2014 Season Were Measured Using a Tipping Bucket Rain Gauge

Sampling time	Precipitation total between sampling times (cm)	Peak precipitation (cm precipitation/10 min)
20 February	21.4	0.32
3 March	8.1	0.27
15 April	9.3	0.30
1 May	3.9	0.15

ground samples at 105 °C for 24 hr, and multiplying the C or N concentration by the ratio of weight of air-dried sample by the weight of oven-dried sample.

For the nuclear magnetic resonance (NMR) analyses, a subset of 16 soils and sediments were randomly selected within the different treatment groups and sampling time points, to include three timepoints for each treatment group. This subset of samples was demineralized with a 10% HF and 10% HCl solution, followed by rinsing five times with MilliQ deionized (DI) water to increase the C concentration in the samples as well as to remove minerals and paramagnetic interference from iron and manganese in soil, and thereby improve the signal to noise ratio of the NMR analysis (Gélinas et al., 2001). These demineralized samples, along with the laboratory-charred litter, were analyzed on a 300-MHz Bruker Avance III NMR spectrometer using magic angle spinning and a 4-mm probe spun at 12 kHz. Between 50 and 150 mg of sample was packed into a 4-mm zirconia rotor, which had a frequency of 75 MHz to collect cross polarization spectra. Between 1,600 and 64,000 scans were taken, with a $\geq$2.5 s relaxation delay. Phase and baseline corrections, along with integrations, were completed in Bruker TopSpin software (Version 3.0).

Spectra were integrated into seven regions: 0–45 ppm (alkyl), 45–60 ppm (N alkyl/methoxyl), 60–95 ppm (O-alkyl), 95–110 ppm (di-O-alkyl), 110–145 ppm (aromatic), 145–165 ppm (phenolic), and 165–215 ppm (amide/carboxyl). The percentages from the integrated spectra, constrained by their C and N concentrations, were used to run the six-component molecular mixing model (MMM) to infer biomolecular SOM constituents, including char, or PyC (Baldock et al., 2004; Nelson & Baldock, 2005).

2.4. Statistical Analysis

All sediment, bulk C, N, and isotope data were analyzed for differences across treatment group using mixed linear effects models. We used burn severity and slope degree as fixed effects both with and without interactions. The specific plot number (e.g., HH1) was entered into the models as a random effect to account for the repeated measurements on each sediment fence. Sampling time was utilized separately as a fixed and random effect, depending on whether time was being significance tested. *P* values were obtained using analysis of variance and Tukey honest significant difference test to compare mixed models with empty models that had no fixed effects and were considered significant at $p < 0.05$. Soil data were analyzed using analysis of variance and Tukey honest significant difference tests, since there were no random effects to account for with these samples. No transformations were applied to the data prior to statistical analysis. Data were organized and archived in Microsoft Excel, and all statistical analyses and figures were generated in R (www.r-project.org). NMR data were not analyzed using statistical approaches, due to the small number of spectra collected.

Enrichment ratios (ERs) were calculated by dividing concentrations of C, N, and PyC in eroded sediments with those in the top source soils from 0 to 5 cm for each of the individual sediment fences. However, it is likely that it is only the top centimeter of soil that is eroded, so this calculation may overestimate ERs. An ER greater than one indicates that the sediment has higher concentration of PyC (or C, N) than the source soil and that the PyC (C, N) is being preferentially transported away from its source location compared to other soil constituents.

3. Results

3.1. Source Soils and Mobilized Sediment

Source soils from the Rim Fire area had neutral to basic pH values that ranged from 6.5 to 7.8, and they were significantly dependent on slope classification group and month (χ^2 (5) = 24.538, $p = 0.0001$, Table 2). Source

Table 2
Soil Physical and Chemical Characteristics

Depth	%C	%N	$\delta^{13}C$	$\delta^{15}N$	Bulk density (0–10 cm)	pH in H2O	pH in CaCl2	Sand %	Silt %	Clay %
HH										
0–5 cm	4.48 (1.36)	$0.27\ (0.11)_a$	−25.38 (0.37)	2.10 (0.31)	0.92 (0.02)	6.89 (0.06)	6.68 (0.24)	79.29 (0.66)	13.49 (0.38)	7.20 (0.61)
5–10 cm	3.33 (0.59)	$0.13\ (0.03)_b$	−24.60 (0.19)	3.27 (0.37)	N/A	6.87 (0.06)	5.75 (0.26)	80.54 (0.42)	11.61 (0.32)	7.84 (0.37)
HM										
0–5 cm	4.15 (0.36)	$0.21\ (0.02)_a$	−24.90 (0.19)	3.44 (0.74)	0.95 (0.05)	6.98 (0.14)	6.61 (0.19)	79.44 (1.42)	14.93 (0.44)	5.62 (1.13)
5–10 cm	3.77 (0.37)	$0.15\ (0.00)_b$	−24.65 (0.21)	3.83 (0.34)	N/A	6.97 (0.13)	5.45 (0.13)	77.66 (1.06)	15.60 (0.80)	6.72 (0.57)
MH										
0–5 cm	3.11 (0.80)	$0.11\ (0.02)_a$	−25.15 (0.71)	1.76 (0.26)	0.88 (0.03)	7.09 (0.13)	6.98 (0.09)	80.62 (0.92)	12.37 (1.07)	7.00 (1.00)
5–10 cm	1.52 (0.23)	$0.04\ (0.00)_b$	−24.80 (0.21)	2.45 (0.21)	N/A	6.93 (0.11)	6.14 (0.08)	80.19 (0.59)	12.63 (0.20)	7.16 (0.74)

Note. Parentheses indicate standard error with $n = 3$ analytical replicates. HH = high severity burn, high slope; HM = high severity burn, moderate slope; MH = moderate severity burn, high slope; N/A = not available.
Letters indicate significant differences based on ANOVA and Tukey HSD tests at $p < 0.05$.

soils had C concentrations ranging from 3% to 4%, with the high burn severity sites having nonsignificantly higher C concentration ($p = 0.06$) than the moderate burn severity sites. The C concentration did not vary significantly with depth ($p = 0.12$). The high burn severity classification sites also had almost double the concentration of N compared with the moderate burn severity sites, but this was statistically not significant ($p = 0.06$). However, the N concentration declined significantly with depth ($p = 0.04$).

The mean amount of sediment transported from all sites across all sampling points was 8.2 ± 1.2 g/m^2 per precipitation event (mean ± standard error). The mean amount of sediment transported per precipitation event for the HH, HM, and MH classification groups was 7.1 ± 1.5, 11.9 ± 3.0, and 5.3 ± 0.6 g/m^2, respectively. The most sediment was transported during time periods of greatest precipitation (Table 1 and Figure 4), with February and March having significantly higher ($p = 0.007$, 0.001, 0.001) sediment transport across all sites than April or May. Throughout the sampling period, there were no significant differences in total sediment transported between different burn severity classes ($p = 0.09$) or slope ($p = 0.08$).

Table 3
Sediment Chemical and Physical Characteristics by Treatment Groups: High Burn Severity, High Slope (HH); High Burn Severity, Moderate Slope (HM); and Moderate Burn Severity, High Slope (MH)

Collection date	%C	%N	pH in H_2O	pH in $CaCl_2$	Sand %	Clay %	Silt %
HH							
Feb	$3.45\ (0.48)_a$	$0.18\ (0.02)_a$	$7.47\ (0.11)_a$	$6.79\ (0.10)_a$	83.89 (0.84)	5.92 (0.62)	10.20 (0.68)
Mar	$8.28\ (1.40)_b$	$0.42\ (0.05)_a$	$6.43\ (0.52)_b$	$6.09\ (0.52)_b$	74.21 (2.44)	6.74 (0.99)	19.05 (1.86)
Apr	$8.10\ (1.19)_b$	$0.35\ (0.05)_a$	$7.18\ (0.13)_a$	$6.88\ (0.08)_a$	81.97 (2.09)	6.73 (2.09)	11.31 (1.02)
May	$8.98\ (1.91)_b$	$0.42\ (0.07)_a$	$7.14\ (0.07)_a$	$6.75\ (0.11)_a$	75.11 (4.53)	7.73 (1.21)	17.17 (3.33)
HM							
Feb	$3.42\ (0.62)_a$	$0.19\ (0.03)_b$	$7.58\ (0.06)_a$	$6.96\ (0.10)_a$	78.80 (3.42)	5.93 (1.25)	15.27 (2.80)
Mar	$5.67\ (1.08)_b$	$0.33\ (0.06)_b$	$5.76\ (0.46)_b$	$5.41\ (0.50)_b$	72.23 (5.46)	5.44 (1.56)	22.33 (4.40)
Apr	$4.55\ (0.86)_b$	$0.21\ (0.04)_b$	$7.38\ (0.12)_a$	$6.83\ (0.14)_a$	79.17 (5.07)	6.67 (0.50)	14.15 (5.28)
May	$4.27\ (0.63)_b$	$0.21\ (0.03)_b$	$7.36\ (0.11)_a$	$6.88\ (0.14)_a$	86.07	6.00	7.93
MH							
Feb	$5.77\ (1.97)_a$	$0.17\ (0.06)_b$	$7.37\ (0.07)_a$	$6.53\ (0.13)_a$	83.86 (1.40)	7.49 (1.19)	8.65 (1.30)
Mar	$6.29\ (2.14)_b$	$0.18\ (0.05)_b$	$7.03\ (0.28)_a$	$6.51\ (0.21)_a$	84.00 (1.37)	8.05 (0.46)	7.96 (1.07)
Apr	$7.37\ (1.36)_b$	0.20 (0.03)	$6.60\ (0.21)_a$	$6.40\ (0.12)_a$	87.12 (2.34)	4.46 (3.42)	8.43 (1.08)
May	$5.75\ (0.68)_b$	$0.16\ (0.02)_b$	$7.12\ (0.11)_a$	$6.44\ (0.11)_a$	N/A	N/A	N/A

Note. Means are presented here with standard error by sediment fence included in parentheses ($n = 7$), and those without standard error did not collect enough sediment to conduct replicate analyses. N/A = not available.
Letters indicate significant differences based on ANOVA and Tukey HSD tests at $p < 0.05$.

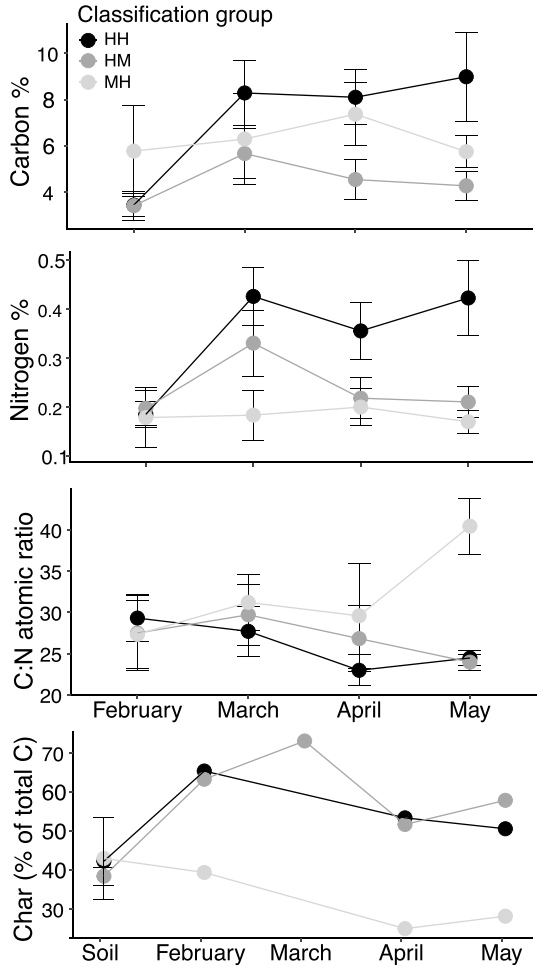

Figure 5. Bulk C (a) and N (b) percentages, and the atomic C:N ratio (c) for the fine (<2 mm) sediment fraction. Error bars represent standard error ($n = 7$), except for pyrogenic carbon (predicted as char by the molecular mixing model), due to limitations in the number of samples able to be analyzed via nuclear magnetic resonance. The sites were divided into three classification groups: high severity burn, high slope (HH); high severity burn, moderate slope (HM); and moderate severity burn, high slope (MH).

The mobilized sediment from high and moderate severity classification areas had slightly lower pH values to the source soils, ranging from 5.4 to 7.4 (Table 3). There were no significant alterations in the pH throughout the sampling period; however, the March sampling point was significantly ($p < 0.01$) lower than the rest of the sampling times. There were no significant differences in the pH between the classification groups ($p = 0.92$–0.99).

There were no significant differences in sand transport between the classification groups ($p = 0.16$–0.22). However, the sand fraction varied significantly by month (χ^2 (5) = 24.272, p = 0.000192), with May having significantly lower sand transport compared with April ($p = 0.001$) and March ($p = 0.001$). May had significantly higher silt transport than any of the other sampling times ($p = 0.001, 0.001, 0.001$). There were no significant differences in the clay fraction with either sampling time or classification group (χ^2 (5) = 2.8871, $p = 0.7174$).

Erosion of the fine sediment fraction (<2 mm) was significantly higher ($p = 0.001$, $p = 0.001$) in February and March than in April or May ($p = 0.001$, $p = 0.001$). The moderate burn severity classification group had significantly less fine fraction transport compared with the high burn severity moderate slope classification group ($p = 0.01$) and was not different from the high burn severity high slope classification group ($p = 0.58$). The coarse fraction was composed of pine needles, pinecones, deciduous leaves, twigs, bark, charcoal, burned materials, and small rocks. The coarse fraction had significantly lower ($p = 0.001, 0.025, 0.001$) transport in the month of May, and the moderate burn severity sites had significantly higher ($p = 0.018, 0.001$) coarse sediment transport than either of the high burn severity classification groups. The moderate burn severity sites still had live and dying trees undergoing needle drop and aerial litter deposition, which served as a major contributor to the coarse sediment fraction (Table 3).

3.2. Carbon and Nitrogen Mobilization

In the sediment, C and N concentrations changed significantly throughout the sampling period, with April having significantly less C than February ($p = 0.001$) and March having significantly more than February ($p = 0.001$, Figure 5), and they were significantly predicted by sampling time and classification group (χ^2 (5) = 24.538, $p = 0.00009$). Average C concentration ranged from 3% to 10%, and the average N concentration ranged from 0.1% to 0.5%. There were no significant differences in C concentrations between the treatment groups ($p = 0.14, 0.89, 0.34$); however, the high severity burn high slope had almost double the concentrations of N compared with the moderate burn severity classification group, which was statistically significant ($p = 0.02$). The atomic C:N ratio for the high severity sites ranged from 18 to 40 and ranged from 19 to 48 in the moderate burn severity sites, and there were no significant trends with classification group or sampling time (χ^2 (5) = 7.6238, $p = 0.1782$).

A comparison of source soil and eroded sediment revealed that the moderate severity classification group had sediment that was enriched (ER > 1) in both C and N compared to the source soil (Figure 6). The sediments from the two high severity classification groups were enriched in C and N compared to their source soils only during the month of March. During the rest of the time points, these higher severity sites were depleted (ER < 1) in C and N compared to source soils.

3.3. Stable Isotope Analyses

The $\delta^{13}C$ from the sediment and soil samples collected from the Rim Fire (Figure 7) ranged from −27‰ to −25‰, and there were no significant ($p = 0.33, 0.14, 0.88$, Figure 7) isotopic changes between the burn and

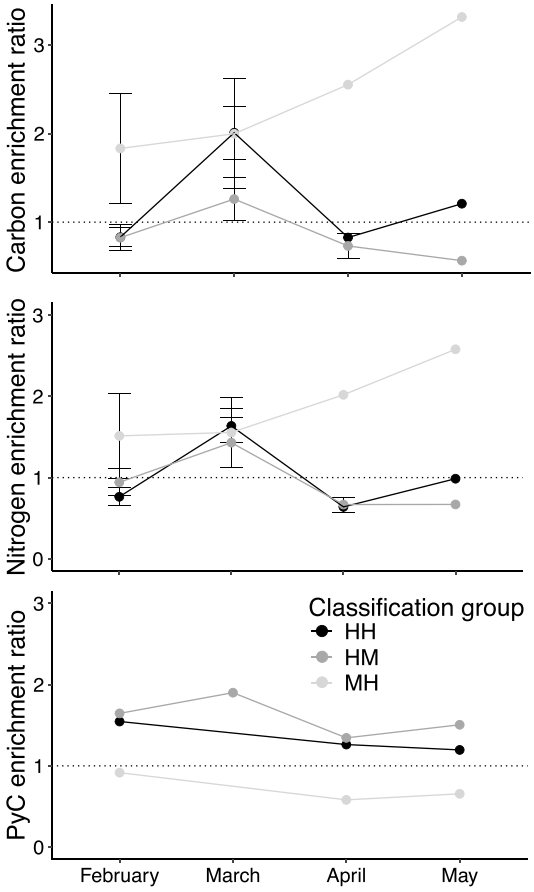

Figure 6. Enrichment ratios for carbon (a), nitrogen (b), and pyrogenic carbon (c) transported sediment (<2 mm). The line at 1 indicates the enrichment line, where >1 is enriched and <1 is depleted in that component. The sites were divided into three classification groups: high severity burn, high slope (HH); high severity burn, moderate slope (HM); and moderate severity burn, high slope (MH).

slope classification groups. There also was one significant difference in $\delta^{13}C$ values between the sampling months, in that February was slightly, but significantly higher than April ($p = 0.03$). The $\delta^{13}C$ of sediments from the medium severity burn were more variable than those from the high severity burn areas. The $\delta^{15}N$ values ranged from −2‰ to 4‰, and February and March values were significantly higher than April ($p = 0.001$, $p = 0.001$), and May was significantly lower than February or March ($p = 0.002$, $p = 0.001$). However, there were significant differences of about 1‰ in the $\delta^{15}N$ values between each of the burn severities, where the HM group was significantly higher than the HH group ($p = 0.001$) and MH was significantly lower than HM and HH ($p = 0.0000$, $p = 0.0000$).

3.4. NMR and MMM Analyses

The NMR analyses of the sediments and soils indicated that the increasing charring temperatures of litter led to significant changes in the chemical composition of the litter (Figure 8 and Table 4), with the lower-temperature char spectrum showing a higher proportion of sugars and aliphatic compounds compared with the high-temperature char, which had a more prominent aromatic peak at 128 ppm. The NMR spectrum from the field collected char from the moderate severity burn area most closely resembles the spectrum from the laboratory *Pinus* litter charred at 250 °C (Figure 8).

The high burn severity soils had higher proportions of alkyl functional groups (16–20%) compared with high burn severity sediments (8–15%), which had 42–50% aromatics compared with the soil range of 32–36% aromatic functional groups (Table 4). The moderate severity burn soils had 30–44% aromatics with 13–24% alkyl functional groups, which the moderate severity burn sediments had a higher proportion of alkyl C, ranging from 13% to 21%, and a lower proportion of aromatics, ranging from 25% to 34%.

The MMM indicated that with increasing charring temperature, the *Pinus* litter lost carbohydrates going from 27% carbohydrates for fresh litter, compared to 1% after charring at 550 °C. Other important changes in litter chemistry with increased charring temperature included loss of lipids, carbonyl groups, and lignin (Table 5). The increased proportion of aromatic functional groups in the charred *Pinus* litter translated to 79.9% of char for the 550 °C temperature. We also observed an increase in the proportion of proteins up to 250 °C, followed by a decline in protein concentration in 550 °C char. The high burn severity sediments had twice as much char-C compared with the moderate severity burn sediments, with lower proportions of carbohydrates and lipids (Table 5). The moderate burn severity sediments had higher proportions of carbohydrates and lower proportions of carbonyl groups and proteins than the high burn severity sediments.

Spectra from sediments in the high severity burn areas (HH and HM) showed consistently higher proportions of aromatic functional groups (i.e., charred remains) compared with their source soils (Figure 9). In contrast, spectra for sediments from the moderate severity burn area (MH) were considerably different than that from HH and HM. Sediments from this treatment group had spectra that contain higher concentrations of presumably fresh, uncharred OM as indicated by the large peak in the O-alkyl region, which represents simple carbohydrates and proteins.

3.5. PyC ERs

Sediments eroded from the high burn severity classification groups (HH and HM) were consistently enriched in PyC, while sediments from the moderate severity burn sediments were consistently depleted

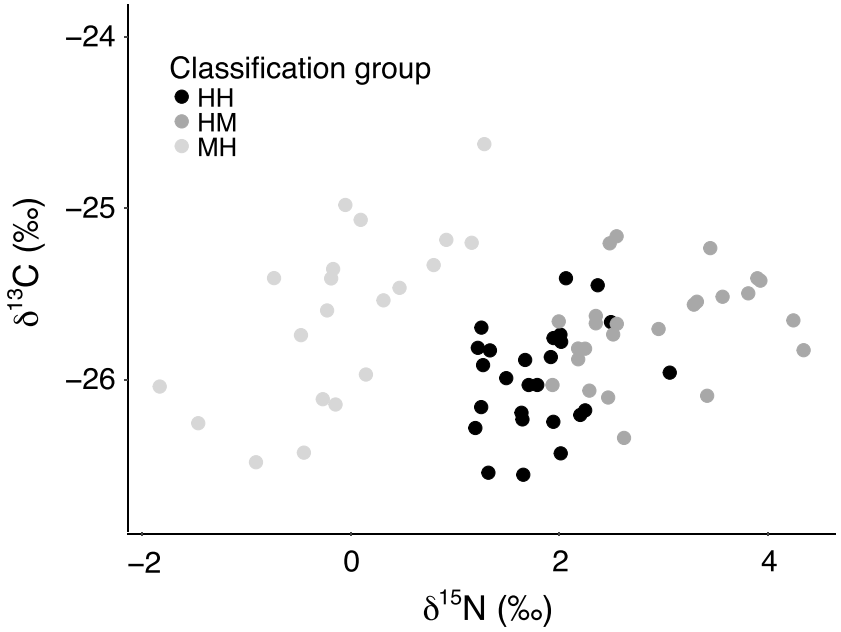

Figure 7. Stable C and N isotopes from the different classification groups in the fine sediment fraction. The high burn severity classification groups (HH and HM) differ from the moderate burn severity (MH) group by enrichment in the $\delta^{15}N$ isotope ratio. There were only small, less than one per mil, differences between the groups across the $\delta^{13}C$ isotope ratio.

in PyC (Figure 6). The ER of PyC in the high burn severity sediments declined throughout the sampling period, although not enough spectra were collected to perform statistical analyses on these data.

4. Discussion

4.1. The Interaction of Fire Intensity and Slope in Controlling Sediment Transport

Erosion-driven transport and redistribution of OM and PyC postfire was controlled by both burn severity and slope after the Rim Fire. The major driver of total sediment transport in our sites along a single hillslope was precipitation intensity, which aligns with the Universal Soil Loss Equation (Wischmeier & Smith., 1965, 1978) and field data (Renard et al., 1997; Robichaud, 2005; Rulli & Rosso, 2005). In sites of moderate burn severity, more coarse litter material was left unconsumed by the fire, leaving more litter available for transport by erosion, which was apparent in the greater coarse fraction transport in the moderate burn severity sites. Conversely, the sites of high burn severity had considerably more soil erosion (<2 mm), likely resulting from a loss of physical stabilization mechanisms, such as aggregation (Albalasmeh et al., 2013; Shakesby & Doerr, 2006), and loss of surface protection from cover by vegetation and litter.

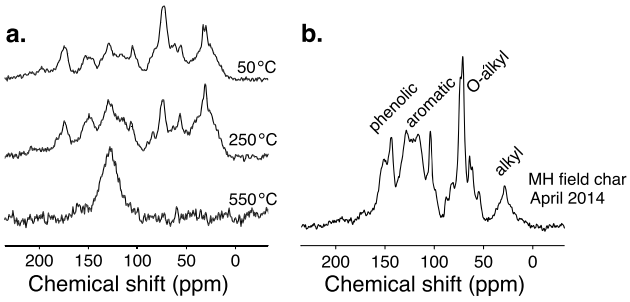

Figure 8. ^{13}C cross polarization magic angle spinning nuclear magnetic resonance comparison of laboratory-produced (a) char produced from litter and Rim Fire char (b). As the laboratory produced char (a) was exposed to increased temperatures, the alkyl, O-alkyl, and phenolic functional groups were lost, and the aromatic region was enhanced. The field char from a moderate burn severity sediment (MH, panel b) site contains higher proportions of aromatic functional groups than the 250 °C char but retained the alkyl and phenolic peaks.

While slope and burn severity can each control the transport of material, in this study site burn severity played a greater role, which is likely reflective of the unprotected and potentially hydrophobic nature of the soils in the high burn severity sites. These exposed soils would have experienced the full force of raindrop impact due to lack of vegetative or litter cover, which can further break down soil aggregates and enhance erodibility of topsoil (Kinnell, 2005; Moody et al., 2013) and associated bulk SOM and PyC. If the moderate burn severity sites had not had a thick litter cover, considerably more sediment transport may have occurred, as has been previously demonstrated with needles,

Table 4
Chemical Functional Group Integrated Regions From ^{13}C NMR Analysis

Sample type	Classification group	Sampling time	Alkyl C	N-alkyl and Methoxyl C	O-alkyl C	Di-O-alkyl C	Aromatic C	Phenolic C	Amide and carboxyl C	Ketone and aldehyde C
			Molar percentage of total organic C							
Pinus duff	50 °C	Nov 2013	20.9	7.7	24.7	7.8	18.6	7.5	9.1	3.6
	250 °C char	Nov 2013	22.7	7.7	15.5	6.9	24.8	10.4	8.8	3.1
	550 °C char	Nov 2013	3.4	1.5	1.2	9.5	61.6	12.9	6.6	3.3
Field char	MH char	Apr 2014	9.6	4.1	24.3	10.3	33.8	12.3	3.7	1.9
Sediment	HH	Feb 2014	8.6	2.8	6.0	7.9	50.1	12.9	9.0	2.9
	HH	Apr 2014	11.7	2.9	10.1	5.6	43.6	13.6	9.4	3.1
	HH	May 2014	15.4	3.9	7.0	4.8	42.6	14.1	9.1	3.1
	HM	Feb 2014	13.0	3.6	4.4	4.6	48.5	13.4	9.6	3.0
	HM	Mar 2014	8.3	1.4	1.9	4.3	53.9	15.1	11.7	3.4
	HM	Apr 2014	10.4	3.3	7.0	5.2	43.5	14.6	11.4	4.5
	HM	May 2014	11.2	3.2	7.1	7.8	47.0	13.8	7.4	2.6
	MH	Feb 2014	17.6	5.6	13.9	6.6	35.6	9.9	7.9	3.1
	MH	Apr 2014	32.0	5.2	15.7	5.7	25.0	8.0	6.5	1.9
	MH	May 2014	22.3	6.1	21.8	7.2	28.1	8.1	4.9	1.5
Soil	HH 0–5 cm	Spring 2014	16.5	4.6	9.0	6.0	36.7	12.5	11.5	3.1
	HH 5–10 cm	Spring 2014	20.0	5.9	12.4	7.0	32.5	10.5	9.1	2.7
	HM 0–5 cm	Spring 2014	19.4	5.1	8.6	4.9	35.6	11.4	11.2	3.8
	HM 0–5 cm	Spring 2014	23.1	5.3	10.2	5.0	32.2	10.0	11.4	2.9
	MH 0–5 cm	Spring 2014	24.0	5.2	12.9	5.4	30.5	9.8	8.9	3.2
	MH 0–5 cm	Spring 2014	13.4	3.3	4.7	5.4	44.8	14.5	10.1	3.9

Note. The classification group indicates the combination of slope and burn severity (HH = high burn severity, high slope, HM = high burn severity, moderate slope, MH = moderate burn severity, high slope) or the temperature of the *Pinus* litter char. NMR = nuclear magnetic resonance.

Table 5
Molecular Mixing Model Results for Each of the Sediments and Chars Analyzed by ^{13}C NMR

Sample type	Classification group	Sampling time	C/N molar ratio	Carbohydrate	Protein	Lignin	Lipid	Carbonyl	Char (PyC)
				percentage of total organic carbon					
Pinus duff	50 °C	Nov 2013	33.0	22.6	11.0	31.0	18.3	6.6	10.4
	250 °C char	Nov 2013	29.8	10.6	12.2	35.8	19.4	4.9	17.1
	550 °C char	Nov 2013	39.3	0.0	0.0	6.9	3.7	6.4	83.0
Field char	MH char	Apr 2014		23.1	0.0	34.1	7.9	2.3	32.5
Sediment	HH	Feb 2014	24.1	4.7	15.1	6.9	3.2	4.7	65.4
	HH	Apr 2014	34.9	7.5	10.4	14.1	8.4	6.2	53.4
	HH	May 2014	24.5	3.0	14.9	16.1	10.9	4.5	50.6
	HM	Feb 2014	18.5	1.7	19.6	4.3	7.1	3.9	63.3
	HM	Mar 2014	19.9	0.0	18.2	0.0	1.8	6.8	73.1
	HM	Apr 2014	28.0	3.5	13.0	17.9	4.9	9.1	51.7
	HM	May 2014	26.1	4.6	13.9	14.6	6.0	2.8	57.9
	MH	Feb 2014	46.8	11.0	7.8	19.5	17.0	5.3	39.4
	MH	Apr 2014	42.0	11.8	8.7	16.8	35.9	1.9	25.0
	MH	May 2014	54.0	19.8	6.7	20.8	23.5	0.9	28.2
Soil	HH 0–5 cm	Spring 2014	17.0	6.1	21.4	15.1	9.5	5.7	42.3
	HH 5–10 cm	Spring 2014	20.8	9.1	15.2	21.3	16.3	4.2	33.9
	HM 0–5 cm	Spring 2014	23.0	5.0	17.5	14.7	15.2	6.8	40.8
	HM 0–5 cm	Spring 2014	24.0	6.6	15.8	14.1	21.0	6.3	36.1
	MH 0–5 cm	Spring 2014	34.5	9.2	10.5	18.1	24.2	5.4	32.5
	MH 0–5 cm	Spring 2014	30.8	0.6	11.8	17.6	9.4	7.1	53.5

Note. The classification group indicates the combination of slope and burn severity (HH = high burn severity, high slope; HM = high burn severity, moderate slope; MH = moderate burn severity, high slope) or the temperature of the *Pinus* litter char. NMR = nuclear magnetic resonance; PyC = pyrogenic carbon.

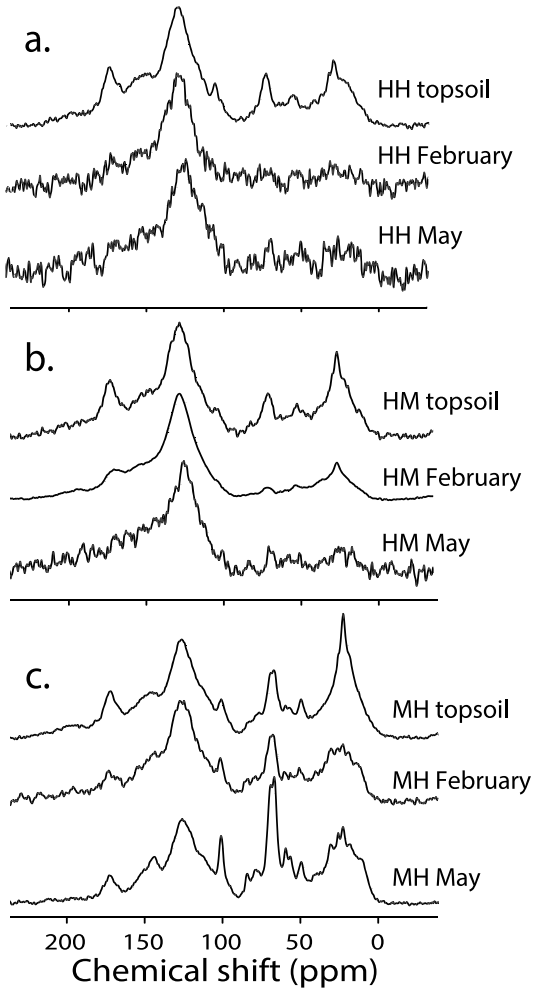

Figure 9. ^{13}C cross polarization magic angle spinning nuclear magnetic resonance spectra of soil organic matter in soil and sediment eroded from the different burn severity and slope classifications. Top soil samples (0–5 cm) are the top lines of the spectra, followed by the first and last sampling points of the 2014 water year. (a) HH indicates high burn severity, high slope. (b) HM indicates high burn severity, moderate slope, and (c) MH indicates moderate burn severity, high slope.

straw, and other OM cover that has been applied to mitigate postfire erosion (Cerdà & Doerr, 2008; Fernández & Vega, 2014; Groen & Woods, 2008; Pannkuk & Robichaud, 2003). However, the presence of litter cover, from both incomplete combustion and needle drop is likely an inherent property of lower-severity burns, and thereby burn severity can act as an environmental trait integrator for understanding postfire erosion. While the formation of a hydrophobic layer was not detected at this site, considerable previous research has demonstrated the role of soil hydrophobicity in contributing to lower infiltration and higher runoff of precipitation, leading to elevated erosion rates in a number of environments, including the Sierra Nevada (Carroll et al., 2007; Doerr et al., 2004; Doerr & Thomas, 2000).

4.2. The Role of Burn Severity in Controlling Soil and Sediment OM Quality

Burn severity played an important role in controlling the amount of both coarse and fine sediment transported after the Rim Fire. Sediment eroded from the moderate severity burn areas was enriched in C and N concentrations compared to their source soils and contained more fresh, organic-rich material than the high severity sites (Figure 6). Greater OM in eroded material from moderate severity burn sites was likely a result of less combustion of fresh OM and postburn needle drop, which was, at least partially, incorporated into the OM of the soil and eroded material through dissolution or fragmentation and downward vertical transport (Cotrufo et al., 2015). This needle drop likely played roles in both contributing to the underlying soil OM pool as well as decreasing the overall sediment export from the moderate severity burn sites.

The high burn severity sites had lower OM and more highly charred material, which is reflected in the relatively enriched ^{15}N value in the high burn severity sediments. This enrichment of ^{15}N with higher burn severity is characteristic of biomass exposed to higher charring intensities, which has been widely reported to impact the $\delta^{15}N$ value of soils (Grogan et al., 2000; E. Huber et al., 2013; Pyle et al., 2015; Saito et al., 2007) by consuming the relatively fresh OM, that is depleted in ^{15}N, on the surface of soil, by selectively consuming ^{14}N during combustion or pyrolysis (Pyle et al., 2015), or by the loss of NH_4^+ compared with NO_3^- (Schmidt & Stewart, 1997). The similarity in the $\delta^{13}C$ value of sediments is expected in soils with the same or similar vegetation, as previous research has indicated that $\delta^{13}C$ typically does not shift with increasing charring temperature (Pyle et al., 2015).

In high severity burn sites, the ERs of C and N were closer to one and more closely resembled the soil mineral material. The high burn severity sites had no remaining live trees to drop needles; thus, mineral material and large woody char fragments dominated the coarse fraction. However, the sediments from these sites were enriched in PyC, whereas the sediments from the moderate burn severity sites were depleted in PyC. This observation suggests that formation temperature of PyC may act as a control on its potential for erosion, which is critical for understanding the fate of PyC within an ecosystem (Mimmo et al., 2014). However, the enrichment of PyC in sediments from the higher burn severity sites may also be due to differences in overall PyC production and interrelated differences in erosion properties in sites experiencing different burn severities. Other research has demonstrated that temperature exhibits a significant control on the properties of PyC, including hydrophobicity, specific surface area, C and N concentration, hydrophobicity, and density, among other properties (Ascough et al., 2008; Mimmo et al., 2014; Santín et al., 2017). These properties likely led to the enhanced erosion of PyC in the high burn severity sites, and depressed erosion of PyC in the moderate burn severity sites.

The moderate and high burn severity sediments differed in terms of OM functional group distribution. The sites that experienced high severity burning had aromatic functional groups constituting approximately 50% more of the OM than the moderate severity burn sites (Table 5). This is consistent with previous findings, which have indicated that with moderate burning, aromatic functional groups may account for between 20% and 30% of the total functional groups and that aromatic functional groups may make up 40–60% of high severity burn sites (Knicker et al., 2006; Mastrolonardo et al., 2015; Miesel et al., 2015; Nave et al., 2011).

Burn severity had a major effect on OM composition, where sediment from moderate severity sites had a higher proportion of carbohydrates and lipids compared to the high severity sites. The composition of OM in moderate severity sites likely reflects the effects of thermal alteration of OM during combustion (Araya et al., 2017) and the input of fresh OM from needle drop postfire. Laboratory charring of *Pinus* litter from the study area showed that the proportion of PyC increased with charring temperature while the proportions of protein and carbohydrate decreased to zero at the highest charring temperature (Table 5). However, our NMR analyses on sediments from high burn severity sites had a higher proportion of protein than the moderate burn severity sites.

The higher than expected concentration of proteins in sediment from high burn severity sites is likely due to a combination of factors. First, it is possible that some topsoil material could have been eroded before the sampling for this study because light ash material can easily be mobilized by wind or water erosion postfire (Pereira et al., 2015) or through vertical mobilization of charred material (Major et al., 2010). Early erosion could lead to the soil and sediment material from sites with high burn severity not closely resembling the laboratory-produced high-temperature char. Other reasons for the soil and sediments not resembling the high-temperature, laboratory-produced char are related to differences in charring conditions, such as lower oxygen availability and longer charring durations in the laboratory (Santín, Doerr, Merino, et al., 2016). However, there was no major formation of rills or gullies during this sampling period and no evidence that the source of the eroded material was from mineral soil, which might be expected to have higher protein contents than highly charred soils and sediments. Second, it is likely that some of the char we collected in eroded sediments came from previous fires, and therefore, its composition more closely resembles microbially processed chars instead of laboratory-produced chars. Large proportions of the land within the boundaries of the Rim Fire had been burned within the past few decades (Van Wagtendonk & Lutz, 2007), and the proportions of PyC in the source soils, even at the deeper sampling depth, are higher than even the 250 °C *Pinus* litter laboratory generated char, which suggests either previous fire history or downward vertical mobilization of PyC. Finally, input of PyC and release of N from previously living biomass (Schmidt & Stewart, 1997) could increase microbial processing in the soil postburn, or the input of vegetative and microbial necromass could have increased concentrations of protein in the soil. Furthermore, we cannot dismiss the possibility that the amount of protein we found in the sediments may be an artifact of the MMM, which was developed for idealized SOM mixtures (Baldock et al., 2004). This biomolecular model may also be overestimating the proportion of char in these samples, as our control laboratory dried litter at 50 °C contained 8% char, which was not consistent with what would be expected for litter samples.

4.3. Implications of OM and PyC Enrichment in Eroded Sediments

The erosional transport and deposition of PyC can lead to significant changes to its environmental persistence (Santín, Doerr, Kane, et al., 2016), particularly due to its potential for preferential erosion, as found after the Rim Fire in this study. The redistribution of PyC throughout a landscape can play a significant role in controlling its long-term persistence in soil. For example, if PyC were to be eroded from the slopes postfire and become stabilized within downslope depositional landform positions, it would likely have greater environmental persistence, particularly if the sediment becomes buried (Chaopricha & Marín-Spiotta, 2014; Marin-Spiotta et al., 2014). Alternatively, PyC may have a shorter residence time, if it becomes exposed to breakdown processes during transport or is transported to a location that has higher decomposition potential than its formation location (Bird et al., 2015). Nevertheless, the enrichment of PyC or C in eroding sediment, such as from high burn severity sites after the Rim Fire, can significantly impact the nutrient budgets of that landscape (Stacy et al., 2015). This preferential erosion can enhance the spatial variability in nutrient distribution throughout a landscape and enhance the difference in nutrient concentration between upslope

eroding landform positions and depositional positions. Additionally, erosional enhancements of PyC concentrations in depositional landform positions can serve to increase soil cation exchange capacity and available nutrients, in addition to sorbing nutrients to enhance nutrient retention (Araya et al., 2016; Johnson et al., 2007). By not accounting for variability in the rates of PyC erosion, considerable error is likely added to field-based estimates of the residence time and fate of PyC in situ (Santín, Doerr, Kane, et al., 2016).

These results suggest that erosive transport of PyC also depends on the burn severity of the landscape wherein the PyC was formed. The combination of combustion intensity as a force for controlling both burn severity and the erosive properties of PyC likely controls the postfire redistribution and fate of PyC over larger scales. Additionally, this relationship suggests that under low and moderate burn severities, the burned area may need less management to retain the PyC, which higher burn severity sites may require more intensive management strategies. Additionally, the soils in this study site were weakly developed Entisols on relatively steep slopes; more developed soils with higher OM input may have more surface roughness that could slow erosion forces, along with enhanced stabilization or breakdown of PyC in situ.

4.4. The Role of Geomorphology in Controlling the Long-Term Fate of PyC

Erosion can dictate the long-term fate of PyC, because eroding and depositional landform positions can exhibit distinct hydrologic and environmental properties that affect decomposition rates for PyC and OM (Abney & Berhe, 2018; Berhe, 2012; Berhe et al., 2008). This effect is potentially enhanced, however, due to the preferential transport of PyC, as we found after the Rim Fire and others have found in experimental burns in agricultural plots (Rumpel et al., 2006). The impact of the landform position on the persistence of C or PyC also depends on whether that material is burned in depositional landform positions, decomposed in situ, or eroded farther down a watershed (Abney & Berhe, 2018). The C storage potential of depositional landform positions can be over 1.6 to 6.2 times that of eroding landform positions (Doetterl et al., 2012). However, because PyC typically has a longer environmental residence time (Boot et al., 2015; Hammes et al., 2008; Lehmann et al., 2008) than nonpyrogenic SOM, this burial-enhanced extended residence time of PyC may be an even more critical factor for controlling its overall environmental persistence.

Over 50,000 ha of the Rim Fire was classified as high burn severity, and over 30,000 ha was classified as moderate burn severity (Potter, 2014). By combining an approximate sediment load of 20 g/m^2/year from the first water year postfire (2013) with the areas impacted by differing burn severities and the mean PyC fraction from moderate and high burn severity treatment groups, erosion could be responsible for the redistribution of over 3,000 and 5,000 Mg of PyC in the first year after the Rim Fire from the moderate burn and high burn severity areas, respectively. This may be a conservative estimate based on higher postfire erosion rates reported in other studies (Carroll et al., 2007; Kirchner et al., 2001; Spigel & Robichaud, 2007). These other studies also likely have different geomorphologic conditions, including slope length, aspect, and angle, along with soil and vegetation types than the landscape impacted by the Rim Fire. However, it is still clear that by not incorporating considerations of gemorphology and how it dictated hillslope level redistribution of PyC into the current understanding of PyC and C cycling, considerable error is being introduced into models of both C and PyC budgets.

4.5. Future Directions and Limitations

The persistence of PyC in soil strongly depends on whether the PyC decomposes in situ or is eroded and subsequently deposited in a site with different decomposition or stabilization potential. The role of landform position on controlling decomposition of SOM has been well described (Berhe, 2012; Doetterl et al., 2012), but this control needs to be assessed for PyC. This study did not address the role of decomposition of PyC during erosional transport, which is a significant process in the breakdown of nonpyrogenic C (Jacinthe & Lal, 2001) or from the soil as a result of leaching (Santos et al., 2016). This study also did not address the fate of PyC after it is deposited. The specific landform position and environmental conditions where PyC is deposited likely play a significant role in its loss from or long-term stability in soil (Abney et al., 2017; Abney & Berhe, 2018). A major limitation of our study is the lack of a moderate burn severity, moderate slope classification group. Without this group, it is impossible to statistically assess interactions between burn severity and slope, though doubtless they exist. This research demonstrates that PyC from high burn severity areas is preferentially erosive; however, the role of slope is unclear in how it controls PyC erosion from soil. Future research should consider the interactions between landscape factors and burn severity,

along with depositional environments and how these environmental factors can control the long-term, landscape-scale persistence of PyC. Understanding the magnitude and controls of PyC fluxes is crucial to understanding the persistence of PyC in soil.

5. Conclusions

Sediment transport during the first year (2014) following the Rim Fire was greatest in the first two postfire study months (February and March), across all combinations of slope and burn severity studied. This higher transport corresponded to higher intensity and total precipitation in these two months compared with the latter two sampling months (April and May). The eroded material from moderate severity burn sites more closely resembled the source soil than the eroded material from the high severity burn sites, and much of this difference was likely due to chemical changes that occurred during combustion or through environmental differences postburning. The sediment from moderate severity burn sites had more inputs of fresh OM than the high burn severity sites, which were depleted in both C and N. However, in the high severity burn sites, the sediment was enriched in PyC and was less similar to its source soil. This enrichment of PyC in only the high burn severity sites suggests that burn severity plays an important role in controlling the quality of OM eroded postfire based on functional group distribution. This preferential erodibility of PyC from these high burn severity sites also indicates that burn severity may play a critical role in determining management strategies for mitigating against postfire erosion and loss of PyC from soil.

Overall, these results illustrate that both the amount and quality of OM and PyC that is eroded postfire is primarily controlled by burn severity and secondarily by geomorphology of the landscape. However, the influence of burn severity, slope, and landform position on the transport of PyC within soil needs further investigation, as these likely interact to control the long-term fate of PyC.

Acknowledgments

The data from this work are available in tables within this work and the following link: https://figshare.com/s/e5be7b443d51337659e8. We would like to acknowledge lab and field work support from Jim Mendez-Lopez and Louis Mielke from the Research Experience for Undergraduates at UC Merced. Lauren Austin, Alicia Sherrin, and technician staff the NPS assisted with collecting samples in the field. We also acknowledge members of the Fogel Stable Isotope laboratory at UC Merced, especially Christina Bradley and David Araiza, for their assistance conducting elemental and stable isotope analyses of sediments and soils. We thank Stephen C. Hart and Jonathan Sanderman for helpful comments on earlier versions of this manuscript. This work was funded by the National Science Foundation (CAREER, EAR 1352627) and the National Park Service (Cooperative agreement P14AC00760) grants to A. A. B. The authors have declared that no competing interests exist.

References

Abney, R., Sanderman, J., Johnson, D., Fogel, M., & Berhe, A. (2017). Post-wildfire erosion in mountainous terrain leads to rapid and major redistribution of soil organic carbon. *Frontiers in Earth Science*, *5*, 99. https://doi.org/10.3389/feart.2017.00099

Abney, R. B., & Berhe, A. A. (2018). Pyrogenic carbon erosion: Implications for stock and persistence of pyrogenic carbon in soil. *Frontiers in Earth Science*, *6*, 26. https://doi.org/10.3389/feart.2018.00026

Albalasmeh, A. A., Berli, M., Shafer, D. S., & Ghezzehei, T. A. (2013). Degradation of moist soil aggregates by rapid temperature rise under low intensity fire. *Plant and Soil*, *362*(1-2), 335–344. https://doi.org/10.1007/s11104-012-1408-z

Araya, S., Meding, S., & Berhe, A. (2016). Thermal alteration of soil physico-chemical properties: A systematic study to infer response of Sierra Nevada climosequence soils to forest fires. *The Soil*, *2*(3), 351–366. https://doi.org/10.5194/soil-2-351-2016

Araya, S. N., Fogel, M. L., & Berhe, A. A. (2017). Thermal alteration of soil organic matter properties: a systematic study to infer response of Sierra Nevada climosequence soils to forest fires. *The Soil*, *3*(1), 31–44. https://doi.org/10.5194/soil-3-31-2017

Ascough, P. L., Bird, M. I., Wormald, P., Snape, C. E., & Apperley, D. (2008). Influence of production variables and starting material on charcoal stable isotopic and molecular characteristics. *Geochimica et Cosmochimica Acta*, *72*(24), 6090–6102. https://doi.org/10.1016/j.gca.2008.10.009

Assouline, S., & Ben-Hur, M. (2006). Effects of rainfall intensity and slope gradient on the dynamics of interrill erosion during soil surface sealing. *Catena*, *66*(3), 211–220. https://doi.org/10.1016/j.catena.2006.02.005

Baker, V. R. (1988). Flood erosion. In *Flood geomorphology* (pp. 81–95). New York: John Wiley & Sons. 15 fig, 52 ref

Baldock, J. A., Masiello, C. A., Gelinas, Y., & Hedges, J. I. (2004). Cycling and composition of organic matter in terrestrial and marine ecosystems. *Marine Chemistry*, *92*(1-4), 39–64. https://doi.org/10.1016/j.marchem.2004.06.016

Battin, T., Luyssaert, S., Kaplan, L., Aufdenkampe, A., Richter, A., & Tranvik, L. (2009). The boundless carbon cycle. *Nature Geoscience*, *2*, 598–600.

Berhe, A. A. (2012). Decomposition of organic substrates at eroding vs. depositional landform positions. *Plant and Soil*, *350*(1-2), 261–280. https://doi.org/10.1007/s11104-011-0902-z

Berhe, A. A., Barnes, R. T., Six, J., & Marín-Spiotta, E. (2018). Role of soil erosion in biogeochemical cycling of essential elements: Carbon, nitrogen, and phosphorus. *Annual Review of Earth and Planetary Sciences*, *46*(1), 521–548. https://doi.org/10.1146/annurev-earth-082517-010018

Berhe, A. A., Harden, J., Torn, M., Kleber, M., Burton, S., & Harte, J. (2012). Persistence of soil organic matter in eroding vs. depositional landform positions. *Journal of Geophysical Research*, *117*, G02019. https://doi.org/10.1029/2011JG001790

Berhe, A. A., Harden, J. W., Torn, M. S., & Harte, J. (2008). Linking soil organic matter dynamics and erosion-induced terrestrial carbon sequestration at different landform positions. *Journal of Geophysical Research*, *113*, G04039. https://doi.org/10.1029/2008JG000751

Berhe, A. A., Harte, J., Harden, J. W., & Torn, M. S. (2007). The significance of erosion-induced terrestrial carbon sink. *Bioscience*, *57*(4), 337–346. https://doi.org/10.1641/B570408

Bird, M. I., Wynn, J. G., Saiz, G., Wurster, C. M., & McBeath, A. (2015). The pyrogenic carbon cycle. *Annual Review of Earth and Planetary Sciences*, *43*(1), 273–298. https://doi.org/10.1146/annurev-earth-060614-105038

Blake, G. R., & Hartge, K. H. (1986). Bulk density. In A. Klute (Ed.), *Methods of soil analysis: Part 1—Physical and mineralogical methods* (2nd ed., pp. 425–442). Madison, WI: American Society of Agronomy and Soil Science Society of America.

Bodí, M. B., Martin, D. A., Balfour, V. N., Santín, C., Doerr, S. H., Pereira, P., et al. (2014). Wildland fire ash: Production, composition and eco-hydro-geomorphic effects. *Earth-Science Reviews*, *130*, 103–127. https://doi.org/10.1016/j.earscirev.2013.12.007

Boot, C., Haddix, M., Paustian, K., & Cotrufo, M. (2015). Distribution of black carbon in ponderosa pine forest floor and soils following the High Park wildfire. *Biogeosciences*, *12*(10), 3029–3039. https://doi.org/10.5194/bg-12-3029-2015

Bouyoucos, G. J. (1962). Hydrometer method improved for making particle size analyses of soils. *Agronomy Journal*, *54*, 464–465.

Cain, M., Subler, S., Evans, J., & Fortin, M. (1999). Sampling spatial and temporal variation in soil nitrogen availability. *Oecologia*, *118*(4), 397–404. https://doi.org/10.1007/s004420050741

Carroll, E. M., Miller, W. W., Johnson, D. W., Saito, L., Qualls, R. G., & Walker, R. F. (2007). Spatial analysis of a large magnitude erosion event following a Sierran wildfire. *Journal of Environmental Quality*, *36*(4), 1105–1105. https://doi.org/10.2134/jeq2006.0466

California Data Exchange Center (2016). California Data Exchange Center.

Cerdà, A., & Doerr, S. H. (2008). The effect of ash and needle cover on surface runoff and erosion in the immediate post-fire period. *Catena*, *74*(3), 256–263. https://doi.org/10.1016/j.catena.2008.03.010

Cerdà, A., & García-Fayos, P. (1997). The influence of slope angle on sediment, water and seed losses on badland landscapes. *Geomorphology*, *18*(2), 77–90. https://doi.org/10.1016/S0169-555X(96)00019-0

Certini, G. (2005). Effects of fire on properties of forest soils: a review. *Oecologia*, *143*(1), 1–10. https://doi.org/10.1007/s00442-004-1788-8

Chaopricha, N. T., & Marín-Spiotta, E. (2014). Soil burial contributes to deep soil organic carbon storage. *Soil Biology and Biochemistry*, *69*, 251–264. https://doi.org/10.1016/j.soilbio.2013.11.011

Chaplot, V., & Le Bissonnais, Y. (2000). Field measurements of interrill erosion under different slopes and plot sizes. *Earth Surface Processes and Landforms*, *25*(2), 145–153. https://doi.org/10.1002/(SICI)1096-9837(200002)25:2<145::AID-ESP51>3.0.CO;2-3

Chia, C., Munroe, P., Joseph, S., Lin, Y., Lehmann, J., Muller, D., et al. (2012). Analytical electron microscopy of black carbon and microaggregated mineral matter in Amazonian dark Earth. *Journal of Microscopy*, *245*(2), 129–139. https://doi.org/10.1111/j.1365-2818.2011.03553.x

Cornelissen, G., Gustafsson, Ö., Bucheli, T., Jonker, M., Koelmans, A., & van Noort, P. (2005). Extensive sorption of organic compounds to black carbon, coal, and kerogen in sediments and soils: Mechanisms and consequences for distribution, bioaccumulation, and biodegradation. *Environmental Science & Technology*, *39*(18), 6881–6895. https://doi.org/10.1021/es050191b

Cotrufo, M. F., Boot, C. M., Kampf, S., Nelson, P. A., Brogan, D. J., Covino, T., et al. (2016). Redistribution of pyrogenic carbon from hillslopes to stream corridors following a large montane wildfire. *Global Biogeochemical Cycles*, *30*, 1348–1355. https://doi.org/10.1002/2016GB005467

Cotrufo, M. F., Soong, J. L., Horton, A. J., Campbell, E. E., Haddix, M. L., Wall, D. H., & Parton, W. J. (2015). Formation of soil organic matter via biochemical and physical pathways of litter mass loss. *Nature Geoscience*, *8*(10), 776–779. https://doi.org/10.1038/ngeo2520

DeBano, L. (2000). The role of fire and soil heating on water repellency in wildland environments: A review. *Journal of Hydrology*, *231*, 195–206.

DeBano, L. F., Neary, D. G., & Ffolliott, P. F. (1998). *Fire's effects on ecosystems*. New York: John Wiley and Sons.

Doerr, S. H., Blake, W. H., Shakesby, R. A., Stagnitti, F., Vuurens, S. H., Humphreys, G. S., & Wallbrink, P. (2004). Heating effects on water repellency in Australian eucalypt forest soils and their value in estimating wildfire soil temperatures. *International Journal of Wildland Fire*, *13*(2), 157–163. https://doi.org/10.1071/WF03051

Doerr, S. H., & Thomas, A. D. (2000). The role of soil moisture in controlling water repellency: New evidence from forest soils in Portugal. *Journal of Hydrology*, *231*, 134–147.

Doetterl, S., Berhe, A. A., Nadeu, E., Wang, Z., Sommer, M., & Fiener, P. (2016). Erosion, deposition and soil carbon: A review of process-level controls, experimental tools and models to address C cycling in dynamic landscapes. *Earth Science Reviews*, *154*, 102–122. https://doi.org/10.1016/j.earscirev.2015.12.005

Doetterl, S., Six, J., Van Wesemael, B., & Van Oost, K. (2012). Carbon cycling in eroding landscapes: Geomorphic controls on soil organic C pool composition and C stabilization. *Global Change Biology*, *18*(7), 2218–2232. https://doi.org/10.1111/j.1365-2486.2012.02680.x

Fernández, C., & Vega, J. A. (2014). Efficacy of bark strands and straw mulching after wildfire in NW Spain: Effects on erosion control and vegetation recovery. *Ecological Engineering*, *63*, 50–57. https://doi.org/10.1016/j.ecoleng.2013.12.005

Gélinas, Y., Baldock, J. A., & Hedges, J. I. (2001). Demineralization of marine and freshwater sediments for CP/MAS 13 C NMR analysis. *Organic Geochemistry*, *32*(5), 677–693. https://doi.org/10.1016/S0146-6380(01)00018-3

Gregorich, E., Greer, K., Anderson, D., & Liang, B. (1998). Carbon distribution and losses: Erosion and deposition effects. *Soil and Tillage Research*, *47*(3-4), 291–302. https://doi.org/10.1016/S0167-1987(98)00117-2

Groen, A. H., & Woods, S. W. (2008). Effectiveness of aerial seeding and straw mulch for reducing post-wildfire erosion, north-western Montana, USA. *International Journal of Wildland Fire*, *17*(5), 559–571. https://doi.org/10.1071/WF07062

Grogan, P., Burns, T., & Chapin Iii, F. (2000). Fire effects on ecosystem nitrogen cycling in a Californian bishop pine forest. *Oecologia*, *122*(4), 537–544. https://doi.org/10.1007/s004420050977

Hammes, K., Schmidt, M. W. I., Smernik, R. J., Currie, L. A., Ball, W. P., Nguyen, T. H., et al. (2007). Comparison of quantification methods to measure fire-derived (black/elemental) carbon in soils and sediments using reference materials from soil, water, sediment and the atmosphere. *Global Biogeochemical Cycles*, *21*, GB3016. https://doi.org/10.1029/2006GB002914

Hammes, K., Torn, M. S., Lapenas, A. G., & Schmidt, M. W. I. (2008). Centennial black carbon turnover observed in a Russian steppe soil. *Biogeosciences*, *5*(5), 1339–1350. https://doi.org/10.5194/bg-5-1339-2008

Harden, J. W., Sharpe, J. M., Parton, W. J., Ojima, D. S., Fries, T. L., Huntington, T. G., & Dabney, S. M. (1999). Dynamic replacement and loss of soil carbon on eroding cropland. *Global Biogeochemical Cycles*, *13*(4), 885–901. https://doi.org/10.1029/1999GB900061

Hendershot, W. H., Lalande, H., & Duquette, M. (2008). Soil reaction and exchangeable acidity. In M. R. Carter & E. G. Gregorich (Eds.), *Soil sampling and methods of analysis* (2nd ed., pp. 173–178). Boca Raton, FL: CRC Press.

Huber, E., Bell, T. L., & Adams, M. A. (2013). Combustion influences on natural abundance nitrogen isotope ratio in soil and plants following a wildfire in a sub-alpine ecosystem. *Oecologia*, *173*(3), 1063–1074. https://doi.org/10.1007/s00442-013-2665-0

Huber, N.K., Bateman, P.C., Wahrhaftig, C. (1989). Geologic map of Yosemite National Park and vicinity, California, Miscellaneous Investigations Series I-1874. US Geological Survey.

Hudak, A. T., Robichaud, P., Evans, J. S., Clark, J., Lannom, K., Morgan, P., & Stone, C. (2014). Field validation of Burned Area Reflectance Classification (BARC) products for post fire assessment. USDA Forest Service/UNL Faculty Publication Paper 220.

Imeson, A., & Lavee, H. (1998). Soil erosion and climate change: The transect approach and the influence of scale. *Geomorphology*, *23*(2-4), 219–227. https://doi.org/10.1016/S0169-555X(98)00005-1

Iniguez, J. M., Swetnam, T. W., & Yool, S. R. (2008). Topography affected landscape fire history patterns in southern Arizona, USA. *Forest Ecology and Management*, *256*, 295–303.

Jacinthe, P., & Lal, R. (2001). A mass balance approach to assess carbon dioxide evolution during erosional events. *Land Degradation & Development*, *12*(4), 329–339. https://doi.org/10.1002/ldr.454

Johnson, D., Murphy, J., Walker, R., Glass, D., & Miller, W. (2007). Wildfire effects on forest carbon and nutrient budgets. *Ecological Engineering*, *31*(3), 183–192. https://doi.org/10.1016/j.ecoleng.2007.03.003

Kinnell, P. (2005). Raindrop-impact-induced erosion processes and prediction: a review. *Hydrological Processes*, *19*(14), 2815–2844. https://doi.org/10.1002/hyp.5788

Kirchner, J. W., Finkel, R. C., Riebe, C. S., Granger, D. E., Clayton, J. L., King, J. G., & Megahan, W. F. (2001). Mountain erosion over 10 yr, 10 k.y., and 10 m.y. time scales. *Geology*, *29*, 591.

Knicker, H., Almendros, G., González-Vila, F. J., González-Pérez, J. A., & Polvillo, O. (2006). Characteristic alterations of quantity and quality of soil organic matter caused by forest fires in continental Mediterranean ecosystems: a solid-state 13C NMR study. *European Journal of Soil Science*, *57*(4), 558–569. https://doi.org/10.1111/j.1365-2389.2006.00814.x

Lal, R. (2003). Soil erosion and the global carbon budget. *Environment International*, *29*(4), 437–450. https://doi.org/10.1016/S0160-4120(02)00192-7

Lehmann, J. (2007). Bio-energy in the black. *Frontiers in Ecology and the Environment*, *5*(7), 381–387. https://doi.org/10.1890/1540-9295(2007)5[381:BITB]2.0.CO;2

Lehmann, J., Skjemstad, J., Sohi, S., Carter, J., Barson, M., Falloon, P., et al. (2008). Australian climate–carbon cycle feedback reduced by soil black carbon. *Nature Geoscience*, *1*(12), 832–835. https://doi.org/10.1038/ngeo358

Liu, S., Bliss, N., Sundquist, E., & Huntington, T. (2003). Modeling carbon dynamics in vegetation and soil under the impact of soil erosion and deposition. *Global Biogeochemical Cycles*, *17*(2), 1074. https://doi.org/10.1029/2002GB002010

Major, J., Lehmann, J., Rondon, M., & Goodale, C. (2010). Fate of soil-applied black carbon: Downward migration, leaching and soil respiration. *Global Change Biology*, *16*(4), 1366–1379. https://doi.org/10.1111/j.1365-2486.2009.02044.x

Marin-Spiotta, E., Chaopricha, N. T., Plante, A. F., Diefendorf, A. F., Mueller, C. W., Grandy, A. S., & Mason, J. A. (2014). Long-term stabilization of deep soil carbon by fire and burial during Early Holocene climate change. *Nature Geoscience*, *7*(6), 428–432. https://doi.org/10.1038/ngeo2169

Masiello, C. (2004). New directions in black carbon organic geochemistry. *Marine Chemistry*, *92*(1-4), 201–213. https://doi.org/10.1016/j.marchem.2004.06.043

Mastrolonardo, G., Rumpel, C., Forte, C., Doerr, S. H., & Certini, G. (2015). Abundance and composition of free and aggregate-occluded carbohydrates and lignin in two forest soils as affected by wildfires of different severity. *Geoderma*, *245*, 40–51.

Mataix-Solera, J., Cerda, A., Arcenegui, V., Jordan, A., & Zavala, L. M. (2011). Fire effects on soil aggregation: a review. *Earth-Science Reviews*, *109*(1-2), 44–60. https://doi.org/10.1016/j.earscirev.2011.08.002

Miesel, J. R., Hockaday, W. C., Kolka, R. K., & Townsend, P. A. (2015). Soil organic matter composition and quality across fire severity gradients in coniferous and deciduous forests of the southern boreal region. *Journal of Geophysical Research: Biogeosciences*, *120*, 1124–1141. https://doi.org/10.1002/2015JG002959

Mimmo, T., Panzacchi, P., Baratieri, M., Davies, C., & Tonon, G. (2014). Effect of pyrolysis temperature on miscanthus (Miscanthus× giganteus) biochar physical, chemical and functional properties. *Biomass and Bioenergy*, *62*, 149–157. https://doi.org/10.1016/j.biombioe.2014.01.004

Moody, J. A., Shakesby, R., Robichaud, P., Cannon, S., & Martin, D. A. (2013). Current research issues related to post-wildfire runoff and erosion processes. *Earth-Science Reviews*, *122*, 10–37. https://doi.org/10.1016/j.earscirev.2013.03.004

Mukherjee, A., Zimmerman, A., & Harris, W. (2011). Surface chemistry variations among a series of laboratory-produced biochars. *Geoderma*, *163*(3-4), 247–255. https://doi.org/10.1016/j.geoderma.2011.04.021

Nave, L. E., Vance, E. D., Swanston, C. W., & Curtis, P. S. (2011). Fire effects on temperate forest soil C and N storage. *Ecological Applications*, *21*(4), 1189–1201. https://doi.org/10.1890/10-0660.1

Nearing, M. (1998). Why soil erosion models over-predict small soil losses and under-predict large soil losses. *Catena*, *32*(1), 15–22. https://doi.org/10.1016/S0341-8162(97)00052-0

Neary, D., Klopatek, C., DeBano, L., & Ffolliott, P. (1999). Fire effects on belowground sustainability: A review and synthesis. *Forest Ecology and Management*, *122*(1-2), 51–71. https://doi.org/10.1016/S0378-1127(99)00032-8

Nelson, P. N., & Baldock, J. A. (2005). Estimating the molecular composition of a diverse range of natural organic materials from solid-state C-13 NMR and elemental analyses. *Biogeochemistry*, *72*(1), 1–34. https://doi.org/10.1007/s10533-004-0076-3

Pannkuk, C. D., & Robichaud, P. R. (2003). Effectiveness of needle cast at reducing erosion after forest fires. *Water Resources Research*, *39*(12), 1333. https://doi.org/10.1029/2003WR002318

Parsons, A., Robichaud, P. R., Lewis, S. A., Napper, C., & Clark, J. T. (2010). *Field guide for mapping post-fire soil burn severity* (p. 49). Fort Collins, CO: United States Department of Agriculture, Forest Service, Rocky Mountain Research Station.

Pereira, P., Cerdà, A., Úbeda, X., Mataix-Solera, J., Arcenegui, V., & Zavala, L. (2015). Modelling the impacts of wildfire on ash thickness in a short-term period. *Land Degradation & Development*, *26*(2), 180–192. https://doi.org/10.1002/ldr.2195

Potter, C. (2014). Geographic analysis of burn severity for the 2013 California Rim Fire. *Natural Resources*, *05*(11), 597–606. https://doi.org/10.4236/nr.2014.511052

Pyle, L. A., Hockaday, W. C., Boutton, T., Zygourakis, K., Kinney, T. J., & Masiello, C. A. (2015). Chemical and isotopic thresholds in charring: Implications for the interpretation of charcoal mass and isotopic data. *Environmental Science & Technology*, *49*(24), 14,057–14,064. https://doi.org/10.1021/acs.est.5b03087

Randerson, J. T., Chen, Y., van der Werf, G. R., Rogers, B. M., & Morton, D. C. (2012). Global burned area and biomass burning emissions from small fires. *Journal of Geophysical Research*, *117*, G04012. https://doi.org/10.1029/2012JG002128

Regnier, P., Friedlingstein, P., Ciais, P., Mackenzie, F. T., Gruber, N., Janssens, I. A., et al. (2013). Anthropogenic perturbation of the carbon fluxes from land to ocean. *Nature Geoscience*, *6*(8), 597–607. https://doi.org/10.1038/ngeo1830

Renard, K. G., Foster, G. R., Weesies, G., McCool, D., & Yoder, D. (1997). *Predicting soil erosion by water: A guide to conservation planning with the Revised Universal Soil Loss Equation (RUSLE)*. Washington, DC: US Government Printing Office.

Riebe, C. S., Kirchner, J. W., Granger, D. E., & Finkel, R. C. (2001). Minimal climatic control on erosion rates in the Sierra Nevada, California. *Geology*, *29*(5), 447–450. https://doi.org/10.1130/0091-7613(2001)029<0447:MCCOER>2.0.CO;2

Robichaud, P. R. (2003). Infiltration rates after prescribed fire in Northern Rocky Mountain forests. In C. J. Ritsema & L. W. Dekker (Eds.), *Soil water repellency: Occurrence, consequences, and amelioration* (Vol. 203, pp. 203–211). Amsterdam, Netherlands: Elsevier.

Robichaud, P. R. (2005). Measurement of post-fire hillslope erosion to evaluate and model rehabilitation treatment effectiveness and recovery. *International Journal of Wildland Fire*, *14*(4), 475–485. https://doi.org/10.1071/WF05031

Rulli, M. C., & Rosso, R. (2005). Modeling catchment erosion after wildfires in the San Gabriel Mountains of southern California. *Geophysical Research Letters*, *32*, L19401. https://doi.org/10.1029/2005GL023635

Rumpel, C., Ba, A., Darboux, F., Chaplot, V., & Planchon, O. (2009). Erosion budget and process selectivity of black carbon at meter scale. *Geoderma*, *154*(1-2), 131–137. https://doi.org/10.1016/j.geoderma.2009.10.006

Rumpel, C., Chaplot, V., Planchon, O., Bernadou, J., Valentin, C., & Mariotti, A. (2006). Preferential erosion of black carbon on steep slopes with slash and burn agriculture. *Catena*, *65*(1), 30–40. https://doi.org/10.1016/j.catena.2005.09.005

Rumpel, C., Leifeld, J., Santin, C., & Doerr, S. (2015). Movement of biochar in the environment. In *Biochar for environmental management: Science, technology and implementation* (2nd ed., pp. 283–298). New York: Routledge.

Saito, L., Miller, W. W., Johnson, D. W., Qualls, R., Provencher, L., Carroll, E., & Szameitat, P. (2007). Fire effects on stable isotopes in a Sierran forested watershed. *Journal of Environmental Quality*, *36*(1), 91–100. https://doi.org/10.2134/jeq2006.0233

Saiz, G., Goodrick, I., Wurster, C., Nelson, P. N., Wynn, J., & Bird, M. (2018). Preferential production and transport of grass-derived pyrogenic carbon in NE-Australian savanna ecosystems. *Frontiers in Earth Science*, 5.

Sander, M., & Pignatello, J. J. (2005). Characterization of charcoal sorption sites for aromatic compounds: Insights drawn from single-solute and bi-solute competitive experiments. *Environmental Science & Technology*, *39*(6), 1606–1615. https://doi.org/10.1021/es049135l

Santín, C., Doerr, S. H., Kane, E. S., Masiello, C. A., Ohlson, M., Rosa, J. M., et al. (2016). Towards a global assessment of pyrogenic carbon from vegetation fires. *Global Change Biology*, *22*(1), 76–91. https://doi.org/10.1111/gcb.12985

Santín, C., Doerr, S. H., Merino, A., Bryant, R., & Loader, N. J. (2016). Forest floor chemical transformations in a boreal forest fire and their correlations with temperature and heating duration. *Geoderma*, *264*, 71–80. https://doi.org/10.1016/j.geoderma.2015.09.021

Santín, C., Doerr, S. H., Merino, A., Bucheli, T. D., Bryant, R., Ascough, P., et al. (2017). Carbon sequestration potential and physico-chemical properties differ between wildfire charcoals and slow-pyrolysis biochars. *Scientific Reports*, *7*(1), 11233. https://doi.org/10.1038/s41598-017-10455-2

Santos, F., Russell, D., & Berhe, A. A. (2016). Thermal alteration of water extractable organic matter in climosequence soils from the Sierra Nevada, California. *Journal of Geophysical Research: Biogeosciences*, *121*, 2877–2885. https://doi.org/10.1002/2016JG003597

Schmidt, S., & Stewart, G. (1997). Waterlogging and fire impacts on nitrogen availability and utilization in a subtropical wet heathland (wallum). *Plant, Cell & Environment*, *20*(10), 1231–1241. https://doi.org/10.1046/j.1365-3040.1997.d01-20.x

Schofield, R., & Taylor, A. W. (1955). The measurement of soil pH. *Soil Science Society of America Journal*, *19*(2), 164–167. https://doi.org/10.2136/sssaj1955.03615995001900020013x

Shakesby, R., & Doerr, S. (2006). Wildfire as a hydrological and geomorphological agent. *Earth-Science Reviews*, *74*(3-4), 269–307. https://doi.org/10.1016/j.earscirev.2005.10.006

Sharpley, A. (1985). The selection erosion of plant nutrients in runoff. *Soil Science Society of America Journal*, *49*(6), 1527–1534. https://doi.org/10.2136/sssaj1985.03615995004900060039x

Spigel, K. M., & Robichaud, P. R. (2007). First-year post-fire erosion rates in bitterroot National Forest, Montana. *Hydrological Processes*, *21*(8), 998–1005. https://doi.org/10.1002/hyp.6295

Stacy, E., Hart, S. C., Hunsaker, C. T., Johnson, D. W., & Berhe, A. A. (2015). Soil carbon and nitrogen erosion in forested catchments: Implications for erosion-induced terrestrial carbon sequestration. *Biogeosciences Discussions*, *12*(3), 2491–2532. https://doi.org/10.5194/bgd-12-2491-2015

Stallard, R. (1998). Terrestrial sedimentation and the carbon cycle: Coupling weathering and erosion to carbon burial. *Global Biogeochemical Cycles*, *12*(2), 231–257. https://doi.org/10.1029/98GB00741

Staub, B., & Rosenzweig, C. (1992). Global Zobler soil type, soil texture, surface slope, and other properties. Digital raster data on a 1-degree geographic (lat/long) 180X360 grid., Global ecosystems database version 2.0. Seven independent spatial layers. 561,782 bytes in 16 files. NOAA National Geophysical Data Center, Boulder, CO.

United States Department of Agriculture, N.R.C.S. (2007). Soil survey of Yosemite National Park, California.

Van Oost, K., Quine, T., Govers, G., De Gryze, S., Six, J., Harden, J., et al. (2007). The impact of agricultural soil erosion on the global carbon cycle. *Science*, *318*(5850), 626–629. https://doi.org/10.1126/science.1145724

Van Wagtendonk, J. W., & Lutz, J. A. (2007). Fire regime attributes of wildland fires in Yosemite National Park, USA. *Fire Ecology*, *3*(2), 34–52. https://doi.org/10.4996/fireecology.0302034

Wischmeier, W. H., & Smith, D. D. (1965). *Predicting rainfall-erosion losses from cropland east of the Rocky Mountains—Guide for selection of practices for soil and water conservation. Agr. Handbk. No. 282*. Washington, DC: USDA.

Wischmeier, W. H., & Smith, D. D. (1978). *Predicting rainfall erosion losses, Agr. Handbk. No. 537*. Washington, DC: U.S. Dept. Agr.